materials

MDPI

Article

Adhesion Properties Between Rubber Asphalt Mastic and Aggregate: Verification from Surface Free Energy Theory and Molecular Dynamics

Huajia Yin [1], Shenyang Cao [2,3,*], Fucheng Guo [4,*] and Xu Wu [4]

[1] Gansu Jiayuguan Highway Development Center, Jiayuguan 735100, China; yhj18909474361@hotmail.com
[2] Gansu New Development Investment Group Ltd., Lanzhou 730030, China
[3] School of Civil Engineering, Lanzhou University of Science and Technology, Lanzhou 730050, China
[4] School of Civil Engineering, Lanzhou Jiaotong University, Lanzhou 730070, China; wx18893105922@hotmail.com
* Correspondence: csy0522@hotmail.com (S.C.); fcguo@chd.edu.cn (F.G.)

Abstract

The adhesive properties between rubber asphalt mastic and aggregate are crucial to rubber asphalt mixtures' stability and moisture resistance. This paper employs surface free energy (SFE) theory and molecular dynamics (MD) to examine the bond strength and debonding behavior at the rubber asphalt mastic–aggregate interface. The results showed that the dispersion fraction of RC1.0 was 7.12 mJ/m^2 higher than that of RA, and the limestone mineral powder improved the adhesion properties of rubberized asphalt to aggregate and the anti-stripping properties. SiO_2 and $CaCO_3$ are contributors to the van der Waals and electrostatic forces between rubber asphalt–aggregate, respectively. The high concentration of mineral powder has a bridging effect in rubber asphalt mastic–aggregate. $CaCO_3$ filler is more pronounced in enhancing the adhesion properties of rubber asphalt–aggregate. $CaCO_3$ mineral powder mainly improves the anti-debonding ability of rubber asphalt–aggregate by reducing the thickness of water film between rubber asphalt–aggregate.

Keywords: rubber asphalt mastic; aggregate; surface free energy; molecular dynamics; adhesion properties

check for updates

Academic Editor: Miguel Ángel Sanjuán

Received: 23 May 2025
Revised: 11 June 2025
Accepted: 28 June 2025
Published: 1 July 2025

Citation: Yin, H.; Cao, S.; Guo, F.; Wu, X. Adhesion Properties Between Rubber Asphalt Mastic and Aggregate: Verification from Surface Free Energy Theory and Molecular Dynamics. *Materials* **2025**, *18*, 3115. https://doi.org/10.3390/ma18133115

Copyright: © 2025 by the authors. Licensee MDPI, Basel, Switzerland. This article is an open access article distributed under the terms and conditions of the Creative Commons Attribution (CC BY) license (https://creativecommons.org/licenses/by/4.0/).

1. Introduction

Asphalt pavement undergoes prolonged exposure to environmental factors and traffic loads, leading to various forms of deterioration that significantly reduce its service life [1–3]. Consequently, there is a critical demand for road construction materials that combine high-temperature resistance to permanent deformation with favorable fatigue performance at moderate temperatures. To meet these requirements, numerous asphalt modifiers have been developed and applied [4–6]. Research demonstrates that incorporating an optimal amount of crumb rubber from recycled tires not only fulfills these functional objectives but also offers an environmentally sustainable solution for tire waste management [7–10].

The adhesion properties between asphalt and aggregate play a critical role in determining the moisture stability and long-term durability of asphalt mixtures. Recently, the interfacial bonding behavior of rubberized asphalt and aggregates has gained significant research attention. Guo [11] employed a molecular dynamics approach to analyze the influence of rubber content and aggregate type on the adhesive characteristics of the rubberized asphalt–aggregate interface. Xie et al. [12] demonstrated that styrene-butadiene rubber

(SBR) enhances van der Waals forces at the interface, thereby improving bond strength. Based on surface free energy theory, Li [13] found that rubber modification increases the asphalt's surface energy, dispersive component, and adhesion work, further enhancing its bonding performance. Additionally, Zhang [14], Jiao [15], Chen [16], and Mohamed et al. [17] have contributed to the exploration of adhesion mechanisms in rubberized asphalt–aggregate systems.

Asphalt mastic, a blend of asphalt binder and mineral filler, is a vital component in asphalt mixtures. Studies show that mixture failures often initiate at the mastic–aggregate interface, making interfacial adhesion crucial for moisture resistance and overall durability. Xu [18] demonstrated that SiO_2 nanoparticles enhance bonding by strengthening electrostatic interactions at the interface. Tan [19] used surface free energy theory to systematically assess adhesion between mastic and aggregate, while Zhang [20] employed pull-off tests to study how filler composition affects interfacial bonding. However, research on rubber-modified asphalt mastic remains limited, and conventional testing methods often fall short in explaining the complex adhesion mechanisms in rubberized mastic–aggregate systems.

The existing studies mostly focus on the properties of rubber-modified asphalt itself or the ordinary asphalt–aggregate interface, whereas the present study combines the two and focuses on the composite interface system of rubber-modified asphalt mortar (with mineral filler) and aggregate. This study investigates the synergistic effect of two variables, "mineral filler" and "aggregate type", on the interfacial adhesion of rubber-modified asphalt and reveals the adhesion mechanism of the rubber–filler–aggregate ternary system. Utilizing surface free energy theory, we quantitatively analyze the surface energy components, adhesion work, and debonding energy of mineral fillers in rubberized asphalt systems. Furthermore, molecular dynamics simulations are employed to elucidate the influence of both mineral filler and aggregate types on interfacial adhesion properties, ultimately revealing the fundamental bonding mechanisms at the rubberized mastic–aggregate interface. These findings provide novel insights into the formation of interfacial bond strength, with the complete methodological framework illustrated in Figure 1.

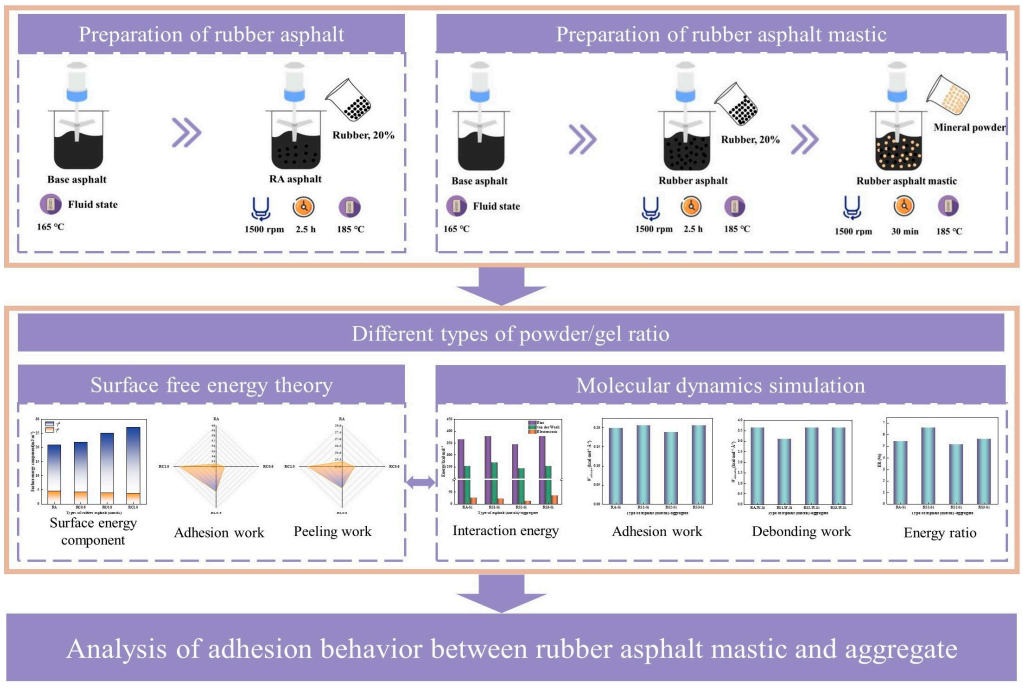

Figure 1. Technical flow chart.

2. Materials and Methods

2.1. Materials

2.1.1. Asphalt Binder

This study utilizes Panjin 90# (penetration grade) as the base material, with its physical properties listed in Table 1.

Table 1. Physical properties of the base asphalt.

Experiment	Requirements	Measured Value
Penetration (25 °C, 100 g, 5 s)/0.1 mm	80–100	89
Ductility 10 °C, 5 cm/min	≥100	>100
Softening point/°C	43–53	45.4
Dynamic viscosity 135 °C/Pa·s	≤3	2.7

2.1.2. Rubber Powder

The physical indices of rubber powder are shown in Table 2.

Table 2. Physical properties of rubber powder.

Experiment	Requirements	Measured Value
Rubber hydrocarbon content (%)	≥42	58
Carbon black content (%)	≥22	31.58
Acetone extract (%)	6–16	8.35
Ash content (%)	≤8	5.13

2.1.3. Mineral Powder

In this work, the mineral powder used is limestone mineral powder, and the relevant test indices are shown in Table 3.

Table 3. Physical properties of mineral powder.

Experiment	Requirements	Measured Value
Relative density (g/cm^3)	≥2.50	2.73
Hydrophilicity coefficient (%)	<1	0.8

The chemical composition and mineralogical composition of the limestone were analyzed using X-ray diffraction (XRD) and X-ray fluorescence spectrometry (XRF), and the results are shown in Figure 2 and Table 4.

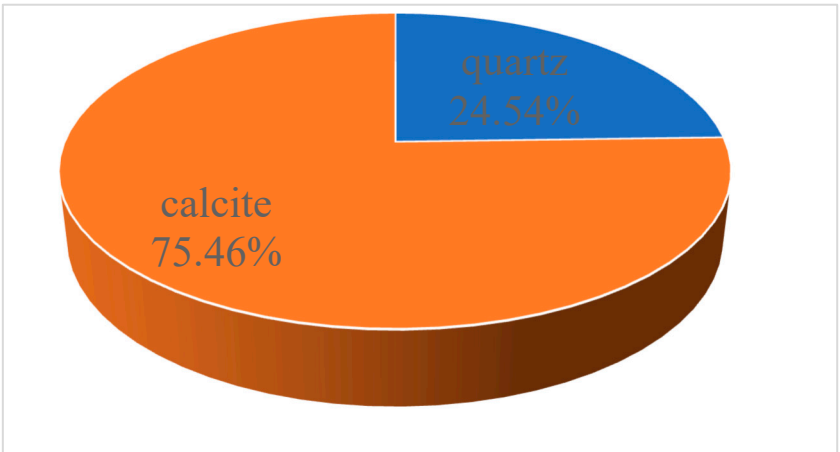

Figure 2. XRD test results for limestone.

Table 4. XRF results of limestone.

Elemental Composition	CaO	SiO_2	MgO	Al_2O_3	K_2O	TiO	MnO	Fe_2O_3	RuO_2
Content/%	52.63	26.56	19.36	0.00	0.00	0.00	0.01	1.10	0.34

From Table 4, it was found that the CaO content and SiO_2 content of the limestone used were 52.63% and 26.56%, respectively. From Figure 2, it was found that quartzite and calcite are the main mineral components of limestone. To minimize the influence of other components, calcite ($CaCO_3$) and quartz (SiO_2) were used as the subjects of this work.

2.2. Preparation of Rubber Asphalt (Mastic)

The preparation process of rubber asphalt and rubber asphalt mastic: ① After the base asphalt was heated to a fluid state at 165 °C, 20% (weight of base asphalt) of the rubber powder was weighed and added to the base asphalt. Stir the asphalt at 185 °C and 1500 rpm for 2.5 h to obtain rubber asphalt. ② A certain amount of mineral powder was weighed and added to the rubber asphalt and was stirred at 1500 r/min for 30 min to obtain different powder-to-gum ratios (0.6, 0.8, and 1.0) of rubber asphalt mastic. The specific preparation process is shown in Figure 3.

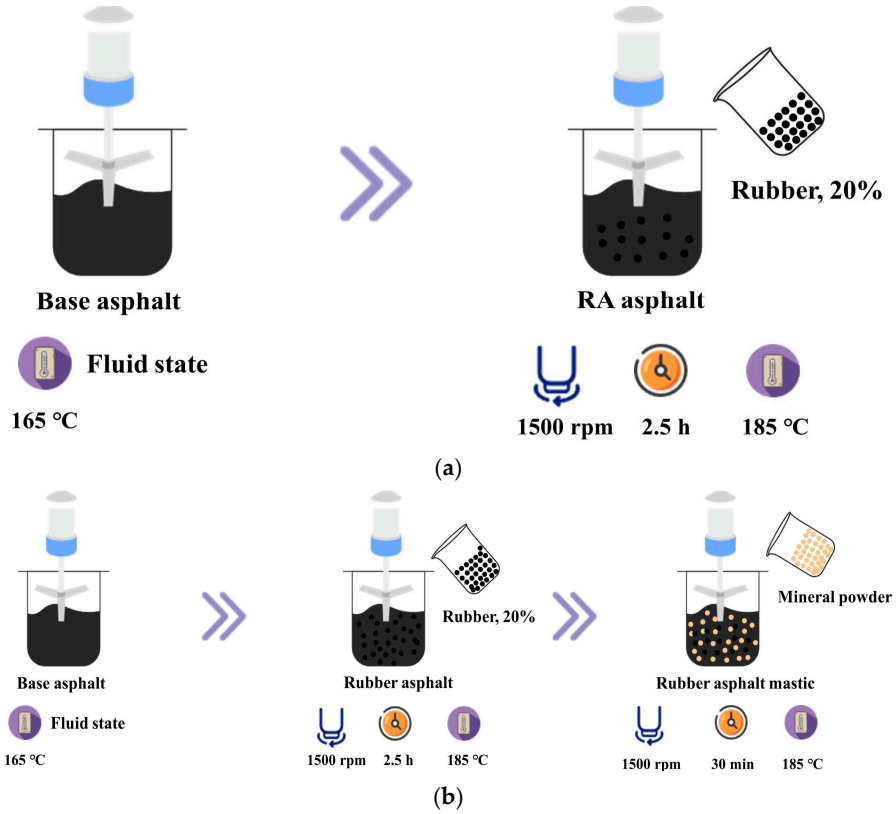

Figure 3. Preparation process of rubber asphalt (mastic) ((**a**): rubber asphalt preparation process; (**b**): rubber asphalt mastic preparation process).

2.3. Surface Free Energy Theory

According to reference [21], Equation (1) mathematically describes the interaction between the polar and dispersive constituents of a material's surface energy.

$$\gamma = \gamma^{\mathrm{d}} + \gamma^{p} = \gamma^{d} + 2\sqrt{\gamma^{+}\gamma^{-}} \quad (1)$$

where γ^p is the polar component, γ^d is the dispersive component, γ^+ is the Lewis acid, and γ^- is the Lewis alkali.

Young's equation (Equation (2)) [22] describes the correlation between the surface energy of asphalt–aggregate systems and their contact angle (θ).

$$\gamma_a \cos\theta = \gamma_s - \gamma_{as} \tag{2}$$

where γ_a is the surface energy of the asphalt binder, γ_s is the surface energy of the aggregate, and γ_{as} is the surface energy of the asphalt mixture.

The interfacial adhesion performance of asphalt and aggregate can be evaluated by the adhesion work (W_{as}), calculated using Equation (3) [23].

$$W_{as} = \gamma_a(1+\cos\theta) = 2\sqrt{\gamma_a^d\gamma_s^d} + 2\sqrt{\gamma_a^+\gamma_s^-} + 2\sqrt{\gamma_a^-\gamma_s^+} \tag{3}$$

The adhesion work (W_{as}) represents asphalt–aggregate bonding in dry conditions, whereas wet conditions typically weaken this interface. The peeling work, defined in Equation (4) [24], quantifies the adhesion under moisture exposure.

$$\begin{aligned} W_{asw} &= 2\sqrt{\gamma_a^d\gamma_w^d} + 2\sqrt{\gamma_s^d\gamma_w^d} + 2\sqrt{\gamma_w^+}\left(\sqrt{\gamma_a^-} + \sqrt{\gamma_s^-}\right) + 2\sqrt{\gamma_w^-}\left(\sqrt{\gamma_a^+} + \sqrt{\gamma_s^+}\right) \\ &\quad -2\gamma_w^d - 2\sqrt{\gamma_a^d\gamma_s^d} - 2\sqrt{\gamma_a^+\gamma_s^-} - 2\sqrt{\gamma_a^-\gamma_s^+} - 4\sqrt{\gamma_w^-\gamma_w^+} \end{aligned} \tag{4}$$

To calculate the surface free energy of asphalt, three solvents: distilled water, glycerin, and formamide are used as known solvents in this paper. The surface energy parameters of the three solvents are shown in Table 5.

Table 5. Test results of the surface energy parameters of the reagents.

Reagent Type	Surface Energy Parameters (mJ/m^2)			
	γ_l	γ_l^d	γ_l^+	γ_l^-
Distilled Water	72.9	21.3	25.8	25.7
Glycerin	65	34	3.96	56.2
Formamide	56	39	2.27	39.5

The surface energy parameters and components of the aggregate are shown in Table 6.

Table 6. Test results of the surface energy parameters of the aggregate.

Aggregate	γ_s	γ^d	γ^p	γ_s^+	γ_s^-
Limestone	34.85	22.55	11.04	1.49	20.45

3. Molecular Dynamics Simulation

3.1. Construction of the Rubber Asphalt Mastic Molecular Model

3.1.1. Molecular Model of Asphalt

The AAA-1 model proposed by Li and Greenfield has been widely used to represent an asphalt binder [11,25], and its rationality and reliability have long been proven [26–28]. Therefore, this paper selects the AAA-1 model to represent the molecular model of the asphalt binder. The 12-component molecular model is shown in Figure 4, and the number of molecules is shown in Table 7.

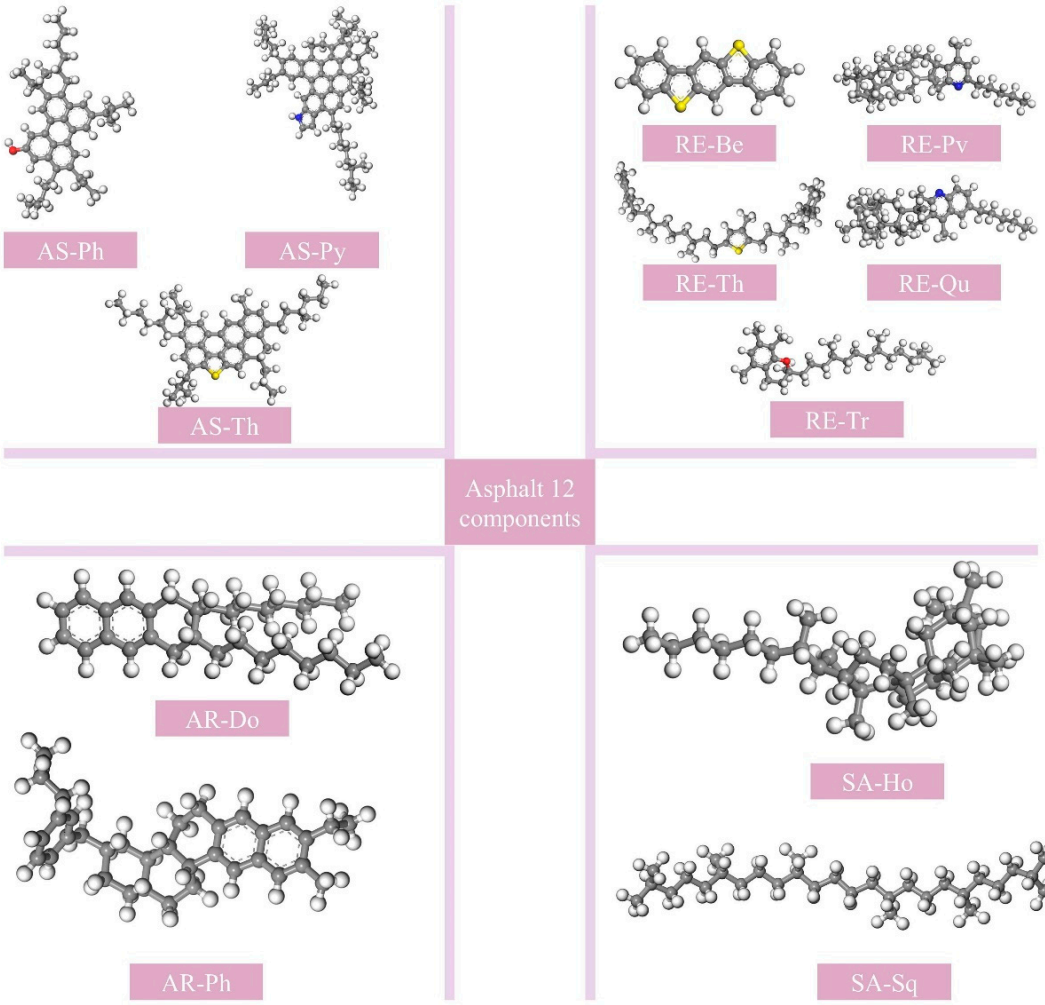

Figure 4. The 12-component molecular model of asphalt.

Table 7. Molecular numbers of the asphalt 12 components.

Type of Component		Molecular Formula	Number of Molecules
Saturate	SA-Ho	$C_{29}H_{50}$	5
	SA-Sq	$C_{30}H_{62}$	4
Aromatic	AR-Do	$C_{30}H_{46}$	18
	AR-Ph	$C_{35}H_{44}$	15
Resin	RE-Be	$C_{18}H_{10}S_2$	15
	RE-Pv	$C_{36}H_{57}N$	4
	RE-Th	$C_{40}H_{60}S$	4
	RE-Qu	$C_{40}H_{59}N$	4
	RE-Tr	$C_{29}H_{50}O$	5
Asphaltene	AS-Ph	$C_{42}H_{54}O$	3
	AS-Py	$C_{66}H_{81}N$	2
	AS-Th	$C_{51}H_{62}S$	3

3.1.2. Molecular Model of Asphalt

In general, rubber tires are mainly composed of natural rubber (NR), butadiene rubber (BR), and styrene-butadiene rubber (SBR), with the largest percentage of natural rubber content [11,29,30]. Therefore, NR is used in this paper to represent the rubber molecule. NR is formed by the polymerization of an isoprene monomer with a polymerization

degree of 24. Figure 5 illustrates the isoprene monomer molecular model and the NR molecular model.

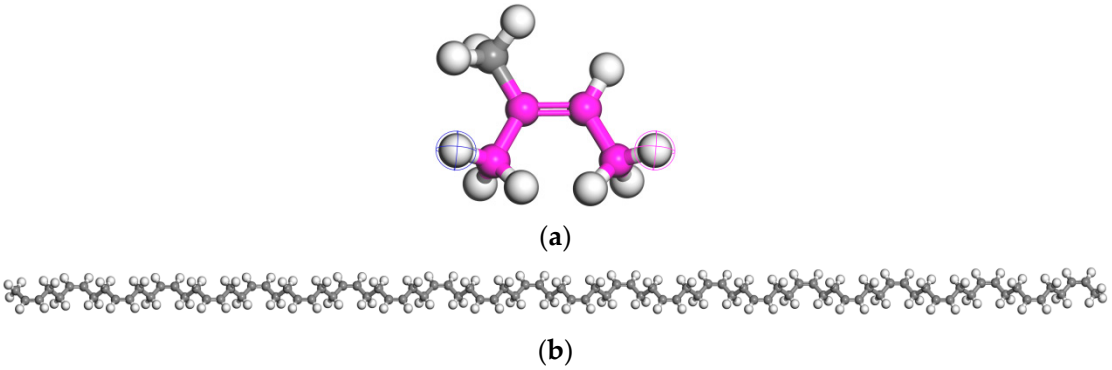

(**a**)

(**b**)

Figure 5. Molecular model of rubber ((**a**): isoprene monomer molecule; (**b**): NR molecule).

3.1.3. Molecular Model of Mineral Powder

Mineral powder is an important component of asphalt mastic. In this paper, the SiO_2 cluster structure and $CaCO_3$ cluster structure are used to represent the most common acidic mineral powders (granite) and alkaline mineral powders (limestone). The crystal parameters of SiO_2 and $CaCO_3$ are shown in Table 8.

Table 8. Crystal parameters of SiO_2 and $CaCO_3$.

Crystal Model	Chemical Formula	Lattice Parameters	Space Group	Group Name
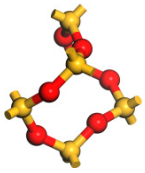	SiO_2	a = b = 4.913 Å c = 5.4052 Å	α = β = 90° γ = 120°	P3121
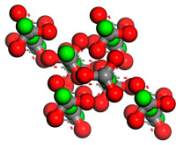	$CaCO_3$	a = b = 4.99 Å c = 17.061 Å	α = β= 90° γ = 120°	R-3C

The SiO_2 and $CaCO_3$ cluster structures were constructed using MS based on the SiO_2 and $CaCO_3$ crystal models in Table 8. The radius of the cluster structure constructed in this paper is 5 Å. Figure 6 shows the construction process of the SiO_2 and $CaCO_3$ cluster structures.

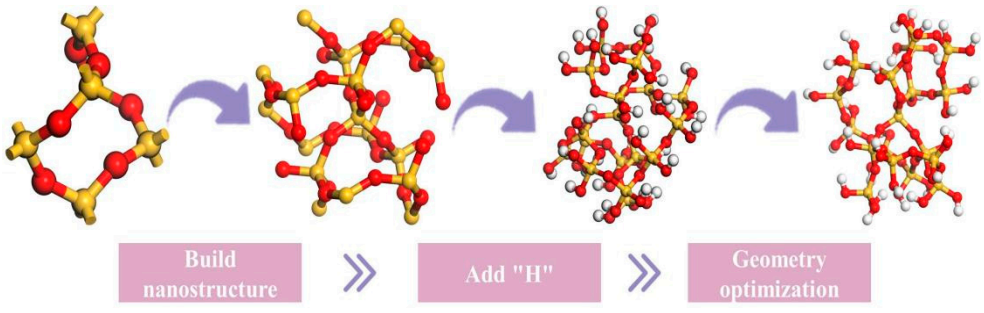

(**a**)

Figure 6. *Cont.*

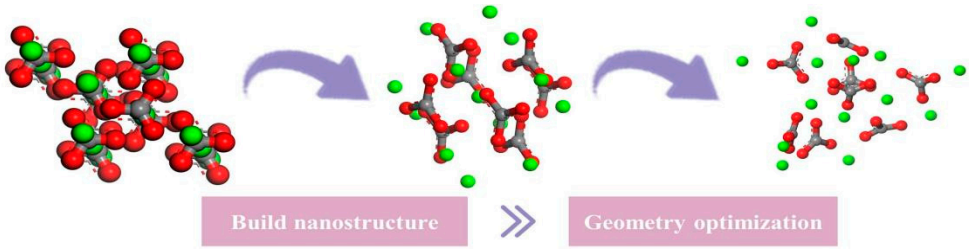

(**b**)

Figure 6. The building process of the mineral powder molecular model ((**a**): SiO_2 cluster structure; (**b**): $CaCO_3$ cluster structure).

3.1.4. Molecular Model of Rubber Asphalt Mastic

The molecular model of the rubber-modified asphalt mastic system was constructed using the amorphous cell module of 2021 MS software. The number of NR molecules, SiO_2 cluster structure molecules, and $CaCO_3$ cluster structure molecules for the molecular model of rubber asphalt mastic are shown in Table 9.

Table 9. Number of NR, $CaCO_3$ cluster structures, and SiO_2 cluster structures in the model of rubber asphalt (mastic).

Type of Asphalt Mastic	Number of Molecules		
	NR	$CaCO_3$ Cluster	SiO_2 Cluster
RA	4	-	-
RS1	4	-	1
RS2	4	-	2
RS3	4	-	3
RC1	4	1	-
RC2	4	2	-
RC3	4	3	-

The rubber asphalt mastic was constructed based on the number of molecules from Tables 1 and 3, as shown in Figure 7.

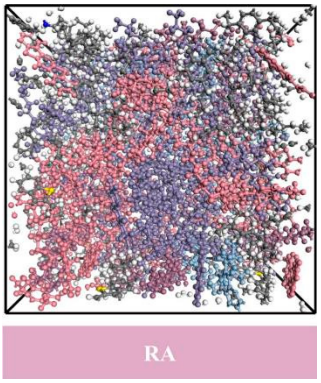

(**a**) Rubber asphalt

Figure 7. *Cont.*

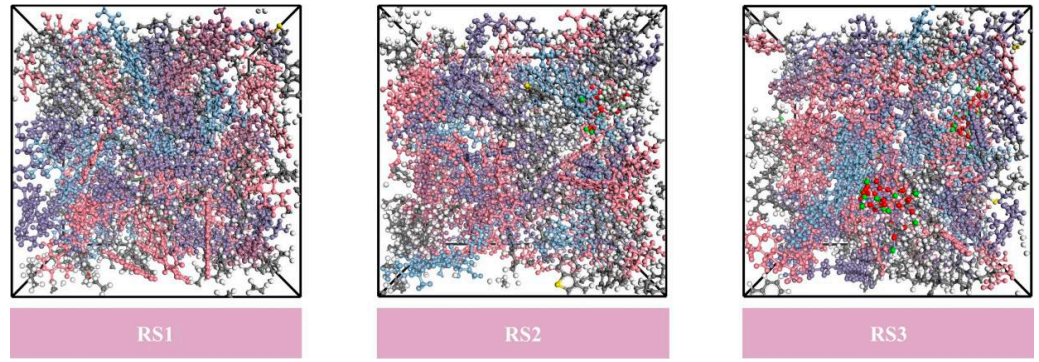

(**b**) Rubber–SiO_2 asphalt mastic

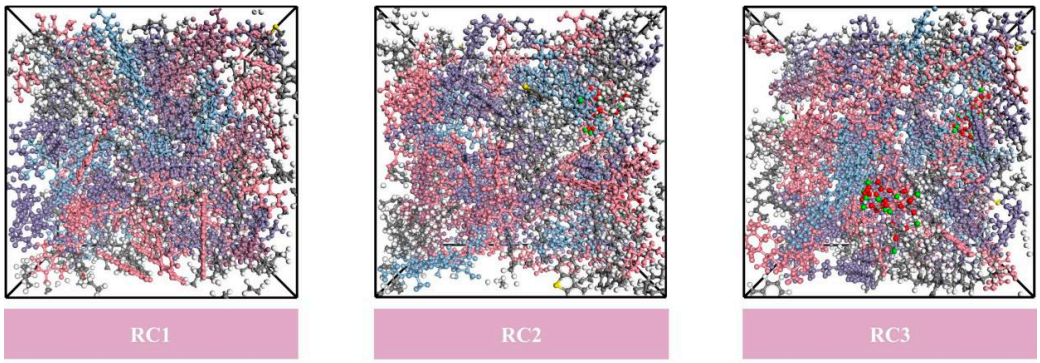

(**c**) Rubber–$CaCO_3$ asphalt mastic

Figure 7. Molecular model of rubber asphalt mastic.

3.2. Construction of the Rubber Asphalt Mastic-Aggregate Molecular Model

The main components of aggregate for road construction contain quartz (SiO_2) and calcite ($CaCO_3$); thus, SiO_2 and $CaCO_3$ are used to represent acidic and alkaline aggregates, respectively. According to the parameters of the SiO_2 and $CaCO_3$ crystals in Table 8, the SiO_2 and $CaCO_3$ 3D models were established. Secondly, the SiO_2 and $CaCO_3$ crystals were cut along the [1, 0, 0] direction. Finally, to make the aggregate layer bonded better with the asphalt mastic layer, the SiO_2 and $CaCO_3$ 3D crystal models were orthogonalized. Figure 8 shows the construction process of the aggregate layer.

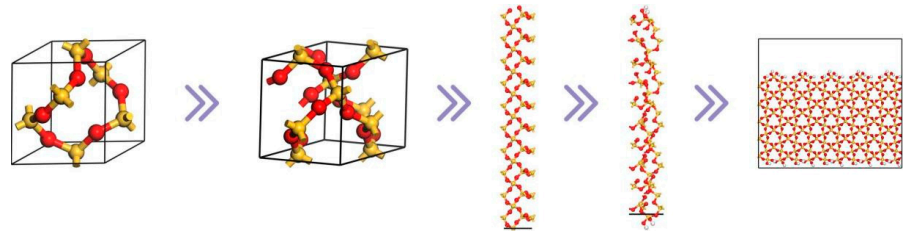

(**a**)

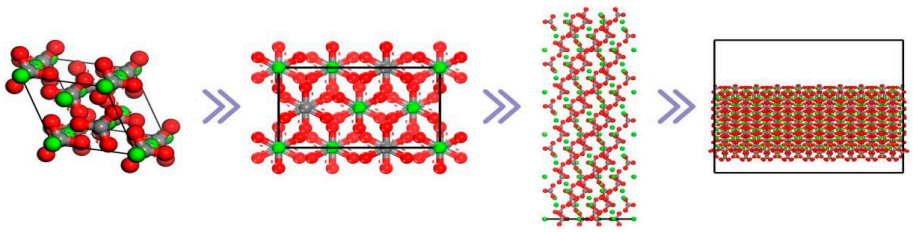

(**b**)

Figure 8. Construction process of the aggregate layer ((**a**) SiO_2 aggregate layer; (**b**) $CaCO_3$ aggregate layer).

The rubber asphalt mastic–aggregate interface model is obtained by adding the rubber asphalt mastic above the aggregate layer. A vacuum layer of 50 Å is added above the rubber asphalt mastic to avoid cyclicity effects. The 3D interface model of rubber asphalt mastic–aggregate is illustrated in Figure 9.

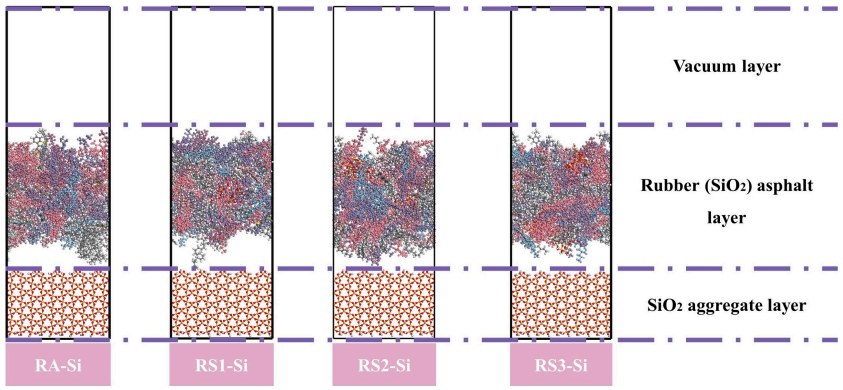

(**a**) Interfacial model of rubber asphalt (SiO_2 mastic)–SiO_2

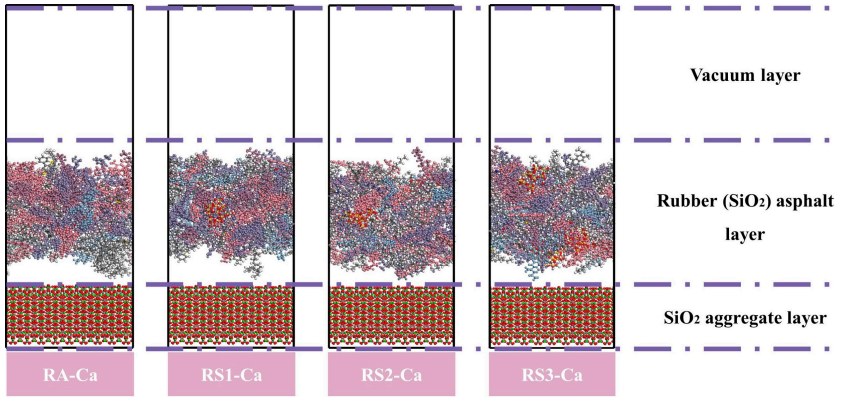

(**b**) Interfacial model of rubber asphalt (SiO_2 mastic)–$CaCO_3$

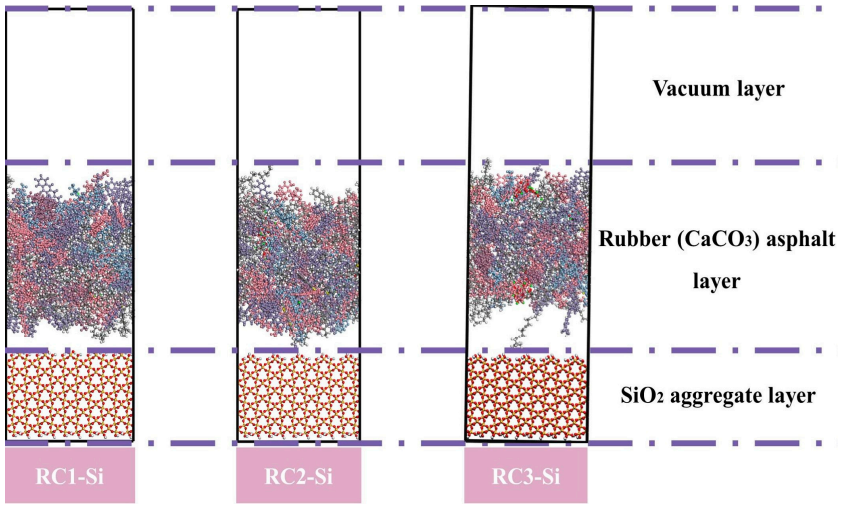

(**c**) Interfacial model of rubber/$CaCO_3$ asphalt mastic–SiO_2

Figure 9. *Cont.*

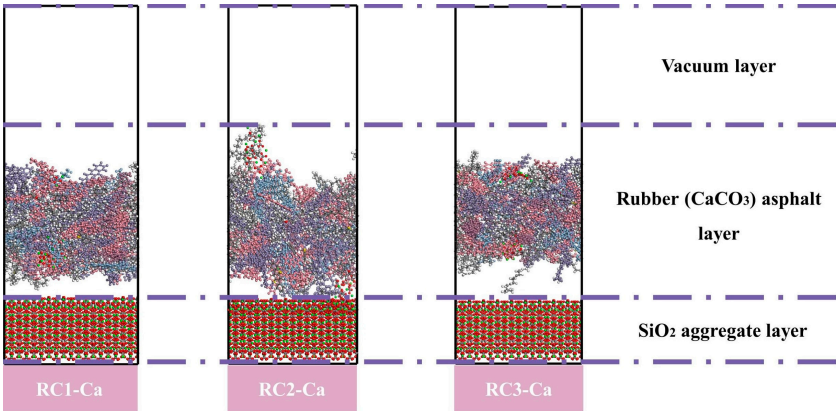

(**d**) Interfacial model of rubber/$CaCO_3$ asphalt mastic–$CaCO_3$

Figure 9. Interface model of rubber asphalt mastic–aggregate.

3.3. Rubber Asphalt Mastic–Water–Aggregate Interface Molecular Model

This study constructed a three-layer interface model of rubber asphalt mastic–water–aggregate to examine the debonding behavior between rubber asphalt mastic and aggregate in the presence of water, as shown in Figure 10.

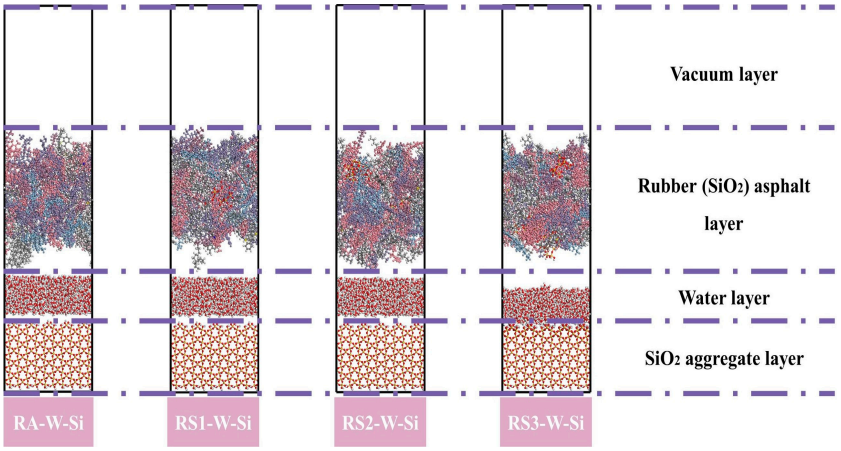

(**a**) Interfacial model of rubber asphalt (SiO_2 mastic)–water–SiO_2

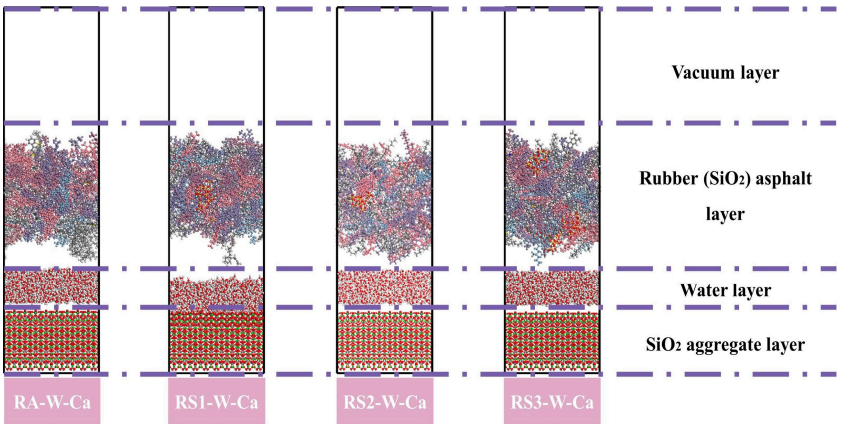

(**b**) Interfacial model of rubber asphalt (SiO_2 mastic) –water–$CaCO_3$

Figure 10. *Cont.*

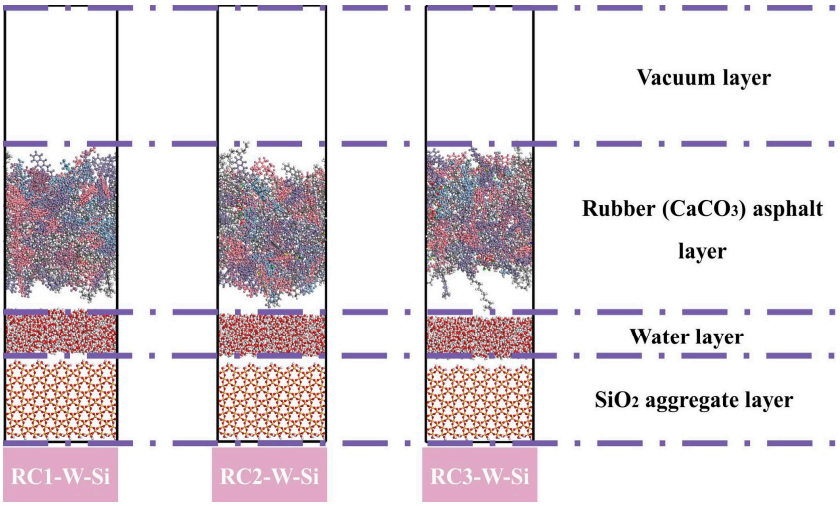

(**c**) Interfacial model of rubber/$CaCO_3$ asphalt mastic–water–SiO_2

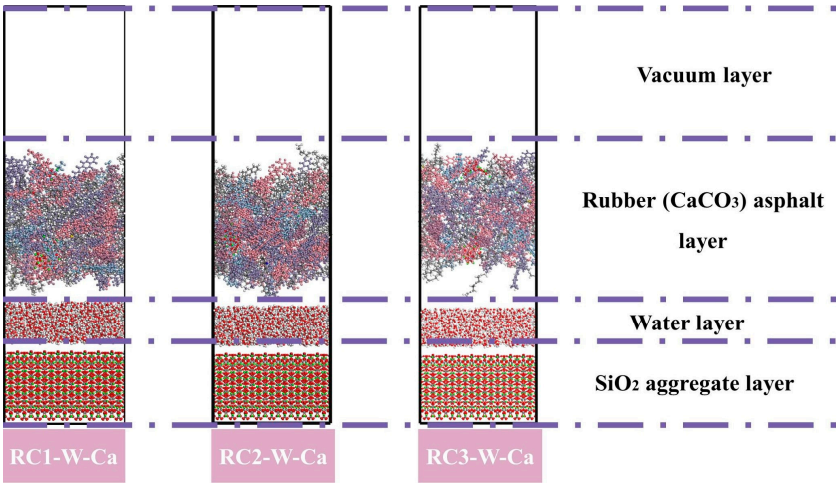

(**d**) Interfacial model of rubber/$CaCO_3$ asphalt mastic–water–$CaCO_3$

Figure 10. Interface model of rubber asphalt mastic–water–aggregate.

3.4. Simulation Methods

This paper used Materials Studio (version 2021) throughout to perform molecular dynamics calculations. This study accomplished the molecular dynamics simulation process under 500 ps NVT conditions. It should be noted that the selected force field in this paper is the COMPASS II force field [18,31,32], and the whole simulation is carried out at 298 K. It should be noted that, in order to ensure the accuracy of the results, the simulation is repeated three times for all models in this paper, and the results are averaged.

3.5. Evaluation Indicators

3.5.1. Adhesive Work

The adhesion work represents the energy required to separate the asphalt from the aggregate surface, which is calculated as shown in Equation (5) [33].

$$W_{adhesion} = -\frac{E_{int}}{A} = -\frac{E_{as} + E_{ag} - E_{as+ag}}{A} \quad (5)$$

where W_{adhesion} is the adhesion work, E_{int} is the interaction energy between asphalt and aggregate, E_{as} is the potential energy of asphalt, E_{ag} is the potential energy of aggregate, $E_{\text{as+ag}}$ is the potential energy of the interface between asphalt and aggregate, and A is the area of contact between asphalt and aggregate interface.

3.5.2. Debonding Work

The presence of water at the asphalt–aggregate interface makes it easier for the asphalt to separate from the aggregate interface. This paper uses debonding work to evaluate the bonding characteristics between asphalt and aggregate in the presence of water, as shown in Equation (6) [34].

$$W_{debonding} = -\frac{E_{as-wa} + E_{ag-wa} - E_{as-ag}}{A} \quad (6)$$

where $W_{debonding}$ is the debonding work, $E_{as–wa}$ is the interaction energy between asphalt and water, $E_{ag–wa}$ is the interaction energy between aggregate and water, and $E_{as–ag}$ is the interaction energy between asphalt and aggregate.

3.5.3. Energy Ratio (ER)

It has been shown that the energy ratio (ER) can represent the ability of the asphalt–aggregate interfacial system to resist moisture damage, as shown in Equation (7) [35].

$$ER = \left| \frac{W_{adhesion}}{W_{debonding}} \right| \quad (7)$$

4. Results and Discussion

4.1. Results Analysis of Surface Free Energy

4.1.1. Surface Energy Component

Figure 11 demonstrates the surface energy of rubber asphalt (mastic) and its components. In Figure 11, the dispersive component of rubber asphalt increases gradually with the increase in mineral powder content. The dispersive components of RA, RC0.6, RC0.8, and RC1.0 are 16.25 mJ·m^{-2}, 17.51 mJ·m^{-2}, 21.11 mJ·m^{-2}, and 23.37 mJ·m^{-2}, respectively. In contrast, the polar component of rubber asphalt decreases with the increasing mineral powder content. The polar components of RA, RC0.6, RC0.8, and RC1.0 are 4.58 mJ·m^{-2}, 4.29 mJ·m^{-2}, 3.97 mJ·m^{-2}, and 3.79 mJ·m^{-2}, respectively. The experimental results demonstrate that the limestone mineral filler significantly enhances the surface energy of rubber-modified asphalt. This improvement stems from the calcite ($CaCO_3$) composition of limestone, where the charged $CaCO_3$ surface facilitates asphalt molecule adsorption through electrostatic interactions. This interfacial phenomenon substantially increases the dispersive component of the rubberized asphalt system [36].

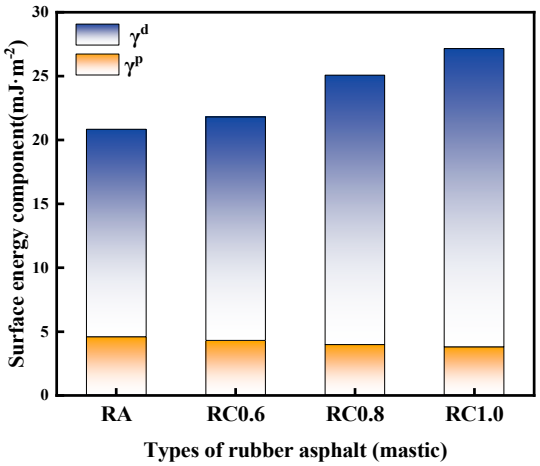

Figure 11. Calculated results of the surface energy and its components (Note: RC0.6, RC0.8, and RC1.0 represent rubber asphalt mastic with a powder/asphalt ratio of 0.6, 0.8, and 1.0, respectively).

4.1.2. Adhesion Work

Adhesion work is an indication of the adhesion properties of the asphalt and aggregate system. The greater the work of adhesion, the better the adhesion between the asphalt and aggregate. The adhesion work for RA, RC0.6, RC0.8, and RC1.0 was calculated according to Equation (3), and the results are shown in Figure 12.

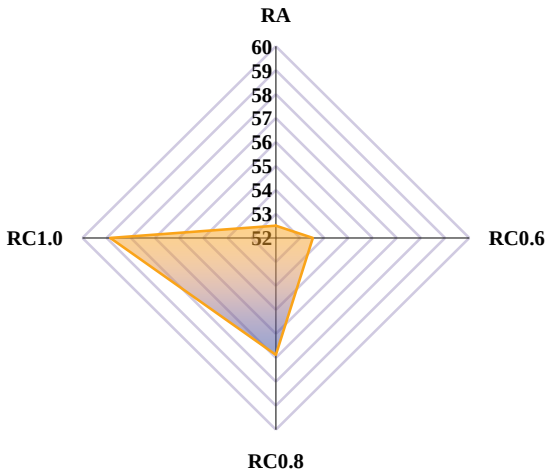

Figure 12. Calculated results of the adhesion work.

Figure 12 shows the adhesion work for RA, RC0.6, RC0.8, and RC1.0, respectively. The adhesion work of RA, RC0.6, RC0.8, and RC1.0 were 52.51 $mJ \cdot m^{-2}$, 53.48 $mJ \cdot m^{-2}$, 56.88 $mJ \cdot m^{-2}$, and 58.85 $mJ \cdot m^{-2}$, respectively. This indicates that mineral powder can effectively improve the adhesion work of rubber asphalt. This further confirms Wang and Pasandín's conjecture [37,38]. After the rubber asphalt mastic is added to the mineral powder, the active sites on the surface of the mineral powder particles come into contact with the asphalt molecules. These sites provide a large number of binding sites, which enhance the physical and chemical bonding between asphalt and mineral powder, thus improving the adhesion work between asphalt and aggregate.

4.1.3. Peeling Work

The peeling work represents the work required to remove the asphalt from the aggregate surface in the presence of water. The greater the peeling work, the more easily the water displaces the asphalt film and the poorer the adhesion of the asphalt and aggregate. The peeling work for RA, RC0.6, RC0.8, and RC1.0 was calculated according to Equation (4), and the results are shown in Figure 13.

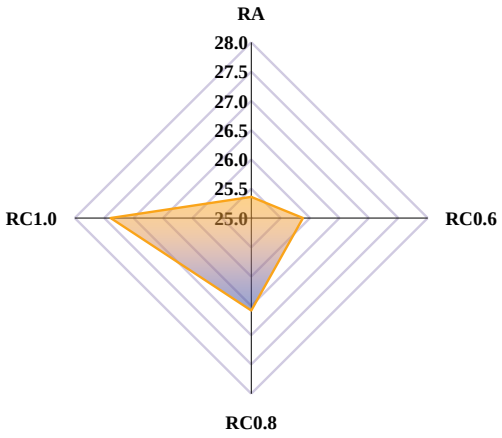

Figure 13. Calculated results of the peeling work.

4.2. Interaction Energy Between Rubber Asphalt (Mastic)–Aggregate

The interaction energy consists of chemical bonding energy and non-bonded forces. The non-bonding energy consists of van der Waals forces and electrostatic interactions [39,40]. Figure 14 illustrates the asphalt–aggregate interface's interaction energy, van der Waals forces, and electrostatic energy.

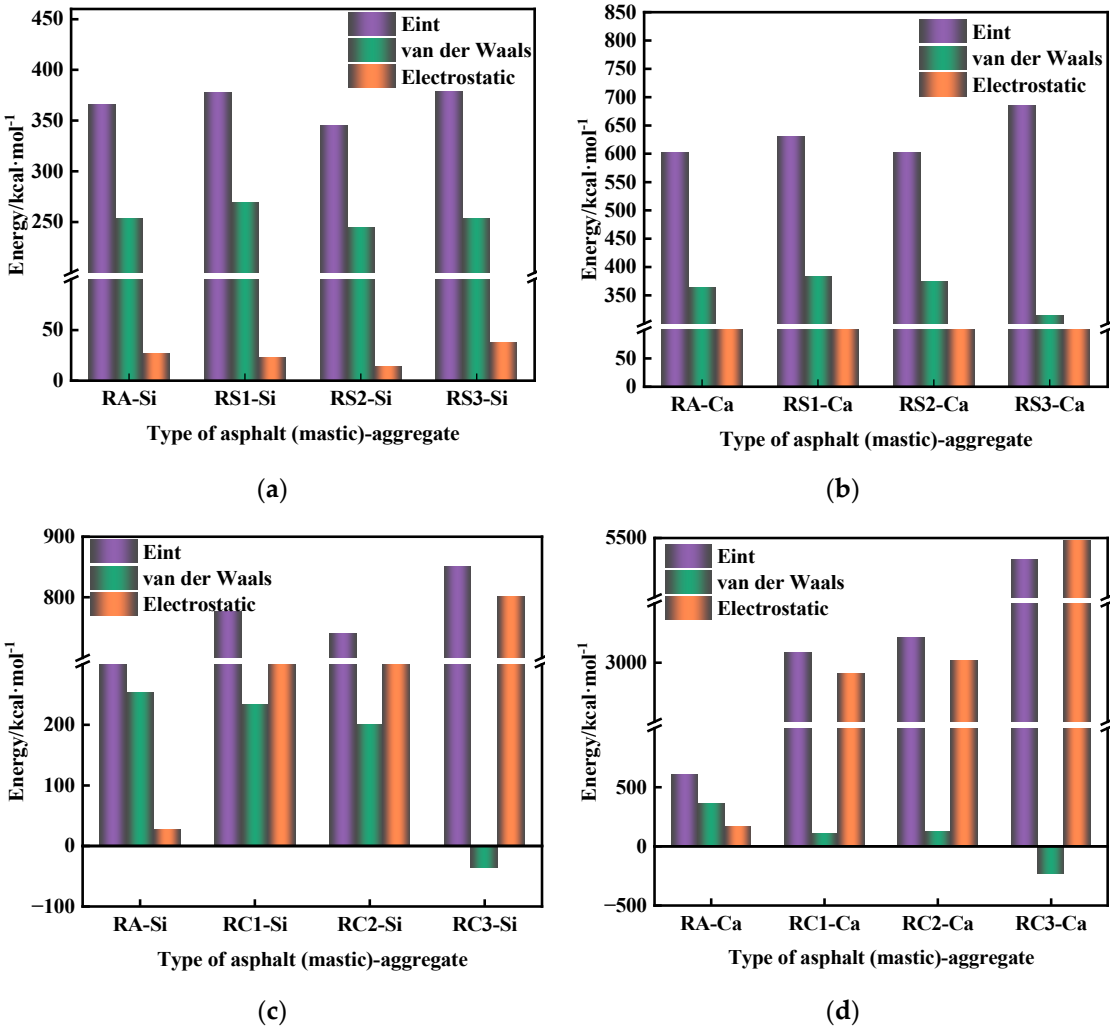

Figure 14. Interaction energy, van der Waals forces, and electrostatic energy of rubber asphalt (mastic)–aggregate. (**a**) Model of the rubber (SiO_2 mineral powder)–SiO_2 aggregate interface, (**b**) model of the rubber (SiO_2 mineral powder)–$CaCO_3$ aggregate interface, (**c**) model of the rubber ($CaCO_3$ mineral powder)–SiO_2 aggregate interface, and (**d**) model of the rubber ($CaCO_3$ mineral powder)–$CaCO_3$ aggregate interface.

Figure 14a,b show the interaction energy, van der Waals force, and electrostatic energy of rubber asphalt (SiO_2 mineral powder)–SiO_2 aggregate and rubber asphalt (SiO_2 mineral powder)–$CaCO_3$ aggregate, respectively. The interaction energy of RA–Si, RS1–Si, RS2–Si, and RS3–Si was 365.929 kcal/mol, 378.169 kcal/mol, 345.5 kcal/mol, and 378.522 kcal/mol, respectively. The interaction energy of RA–Ca, RS1–Ca, RS2–Ca, and RS3–Ca was 602.756 kcal/mol, 630.970 kcal/mol, 602.096 kcal/mol, and 685.446 kcal/mol, respectively. The above results show that the low concentration of the SiO_2 cluster structure can improve the interaction energy between rubber asphalt and aggregate. This may be that a small amount of SiO_2 cluster structure not only increases the surface activity of asphalt but also increases the contact area between rubber asphalt and aggregate, which makes the asphalt and aggregate combine more closely, fills up the tiny pores and unevenness on the

surface of the aggregate, and thus increases the interaction energy between rubber asphalt and aggregate. As the number of SiO_2 cluster structures increases, the interaction energy between rubber asphalt mastic and aggregate is decreased, as shown in Figure 14a,b. As the concentration of SiO_2 cluster increases, the "H" on the surface of these SiO_2 clusters forms hydrogen bonding with asphaltene and resin molecules to form a larger aggregation structure, which impedes the contact between the rubber asphalt and aggregate and reduces the interaction energy between the asphalt mastic and the aggregate. In addition, the high concentration of the SiO_2 cluster structure rather increases the interaction energy between rubber asphalt and aggregate. This is mainly due to the SiO_2 cluster structure forming a bridging effect between the rubber asphalt and aggregate, increasing the van der Waals force between the asphalt mastic and aggregate [41], and then improving the interaction between the asphalt mastic and the aggregate, as shown in Figure 15. These results indicate that the interaction energy between asphalt mastic and aggregate depends on the type of aggregate [42].

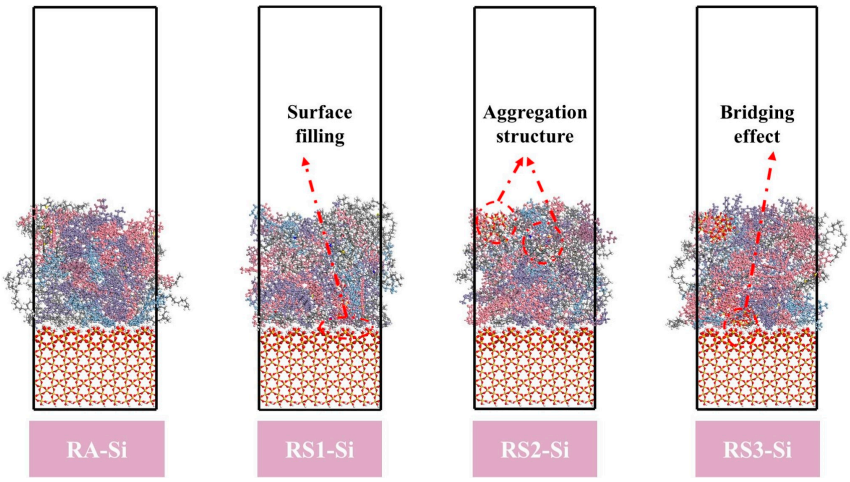

(**a**) Rubber (SiO_2 mineral powder) asphalt mastic–SiO_2 aggregate interfacial conformation

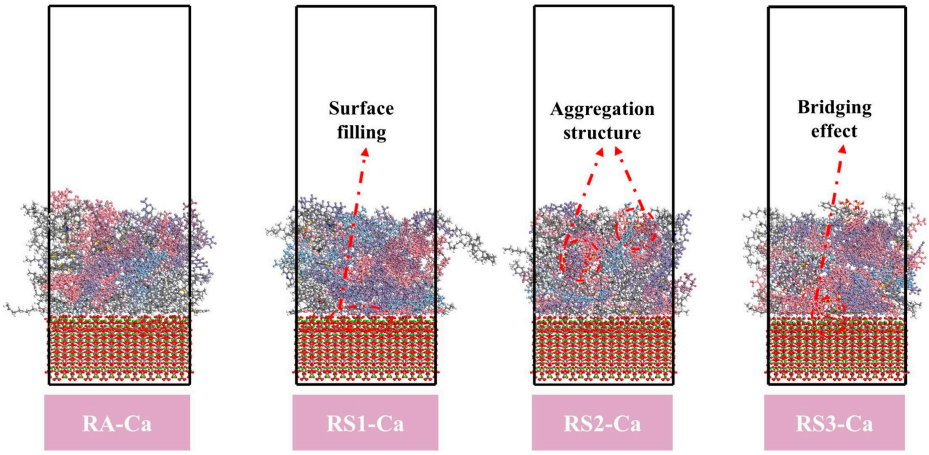

(**b**) Rubber (SiO_2 mineral powder) asphalt mastic–$CaCO_3$ aggregate interfacial conformation

Figure 15. Rubber asphalt mastic–aggregate interfacial conformation.

Figure 14c,d show the interaction energy, van der Waals force, and electrostatic energy of rubber asphalt ($CaCO_3$ mineral powder)–SiO_2 aggregate and rubber asphalt ($CaCO_3$ mineral powder)–$CaCO_3$ aggregate, respectively. The interaction energy of RA–Si, RC1–Si, RC2–Si, and RC3–Si was 365.929 kcal/mol, 776.501 kcal/mol, 740.282 kcal/mol, and 850.202 kcal/mol, respectively. The interaction energy of RA–Ca, RC1–Ca, RC2–Ca, and RC3–Ca was 602.756 kcal/mol, 3083.881 kcal/mol, 3209.635 kcal/mol, and

5319.691 kcal/mol, respectively. For example, compared to RS1–Si and RS1–Ca, RC1–Si and RC1–Ca increased by 105% and 389%, respectively. This is mainly attributed to the presence of carbonate ions in the structure of $CaCO_3$ clusters, which generate electrostatic interactions when they come into contact with asphaltene molecules and resin molecules, enhancing the interaction between the rubberized asphalt and the aggregate.

As for the SiO_2 structure, which is mainly composed of Si-O bonds, the charge distribution is relatively uniform, and its interaction with asphaltene molecules and resin molecules is primarily van der Waals forces, so the interaction between the asphalt mastic and aggregate can be dominated by van der Waals forces, as shown in Figure 14. The van der Waals force between asphalt mastic and aggregate is negative under a high concentration of $CaCO_3$ filler. The van der Waals force of RC3–Si and RC3–Ca are −35.345 kcal/mol and -228.519 kcal/mol, respectively. This phenomenon may be due to the high concentration of $CaCO_3$ and asphalt molecules to form a dense network structure, and $CaCO_3$ acts as a bridge to shorten the contact distance between the asphalt mortar molecules and the aggregate, as shown in Figure 16. In addition, $CaCO_3$ shows high polarity, resulting in the interaction force between asphalt mastic and aggregate being dominated by electrostatic energy. At this time, the van der Waals force exhibits a repulsive effect, resulting in a negative van der Waals force.

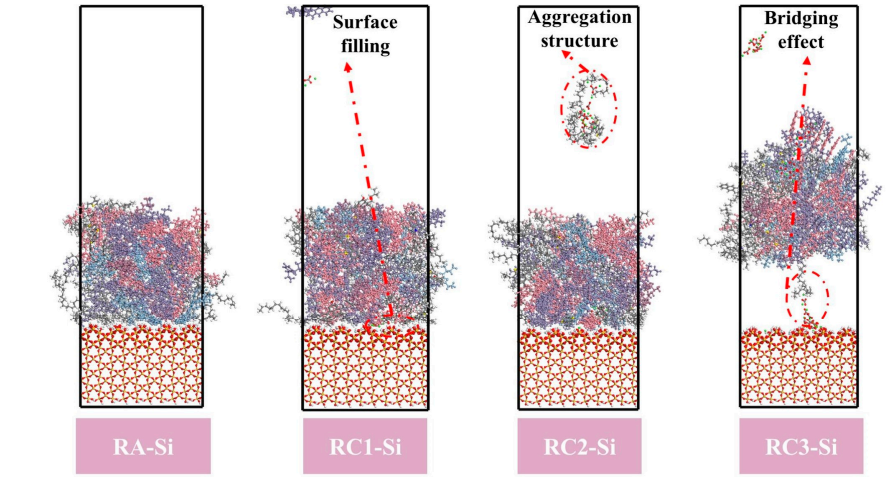

(**a**) Rubber ($CaCO_3$ mineral powder) asphalt mastic–SiO_2 aggregate interfacial conformation

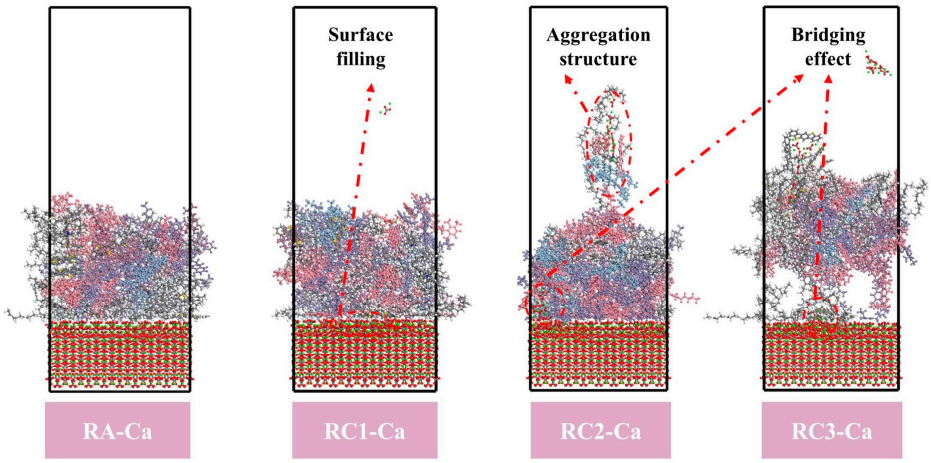

(**b**) Rubber ($CaCO_3$ mineral powder) asphalt mastic–$CaCO_3$ aggregate interfacial conformation

Figure 16. Rubber asphalt mastic–aggregate interfacial conformation.

4.3. Adhesion Behavior Between Asphalt and Aggregate Under Dry Conditions

To evaluate the energy required for the separation of rubber asphalt mastic from the aggregate surface under the dry conditions, the adhesion work of rubber asphalt (mastic) was calculated according to Equation (5). The results of the calculation are shown in Figure 17.

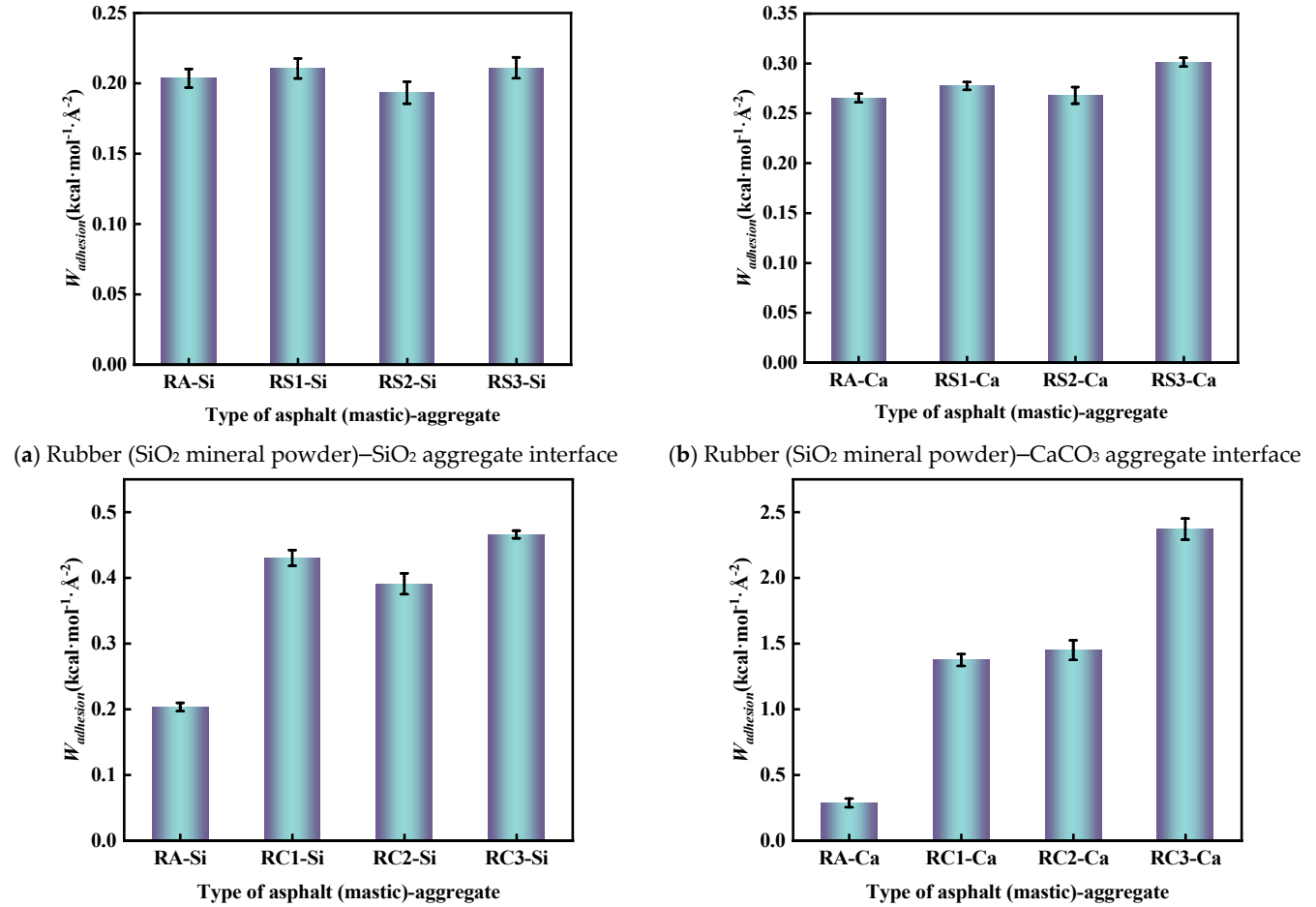

(**a**) Rubber (SiO_2 mineral powder)–SiO_2 aggregate interface (**b**) Rubber (SiO_2 mineral powder)–$CaCO_3$ aggregate interface

(**c**) Rubber ($CaCO_3$ mineral powder)–SiO_2 aggregate interface (**d**) Rubber ($CaCO_3$ mineral powder)–$CaCO_3$ aggregate interface

Figure 17. Adhesion work of the rubber asphalt (mastic)–aggregate.

As can be seen from Figure 17, the adhesion work between rubber asphalt mastic and aggregate was significantly improved by the addition of mineral powder. For example, the adhesion work of RA–Si, RS1–Si, and RC1–Si was 0.20 kcal·mol^{-1}·Å^{-2}, 0.21 kcal·mol^{-1}·Å^{-2}, and 0.42 kcal·mol^{-1}·Å^{-2}, respectively. The adhesion work of RA–Ca, RS1–Ca, and RC1–Ca was 0.26 kcal·mol^{-1}·Å^{-2}, 0.27 kcal·mol^{-1}·Å^{-2}, and 1.34 kcal·mol^{-1}·Å^{-2}, respectively. However, the improvement effect of SiO_2 filler on the adhesion work between rubber asphalt and aggregate is much lower than that of $CaCO_3$ filler. This is because the surface of $CaCO_3$ filler has a positive and negative charge, which can produce a strong electrostatic attraction, significantly enhancing the interfacial bonding strength between asphalt mastic and aggregate. At the same time, the high surface energy of the $CaCO_3$ surface makes it form stronger adhesion with asphalt, which further enhances the adhesion work between rubber asphalt mastic and the aggregate system. In contrast, SiO_2 filler mainly relies on weak van der Waals forces, and its surface chemical inertness makes it less effective in enhancing the adhesion between the rubber asphalt mastic and the aggregate. Therefore, although SiO_2 filler can also enhance the adhesion work, its effect

is inferior to that of $CaCO_3$ filler. Consistent with previous studies, the adhesion work of rubberized asphalt mastic with $CaCO_3$ aggregate is much higher than that of rubber asphalt mastic with SiO_2 aggregate [23,43].

4.4. Debonding Work Between Asphalt and Aggregate Under Wet Conditions

To evaluate the debonding behavior of asphalt from the aggregate surface in the presence of moisture, the debonding work of the rubber asphalt (mastic)–water–aggregate system was calculated using Equation (6), the results are shown in Figure 18. The greater the debonding work, the easier it is to be destroyed by moisture.

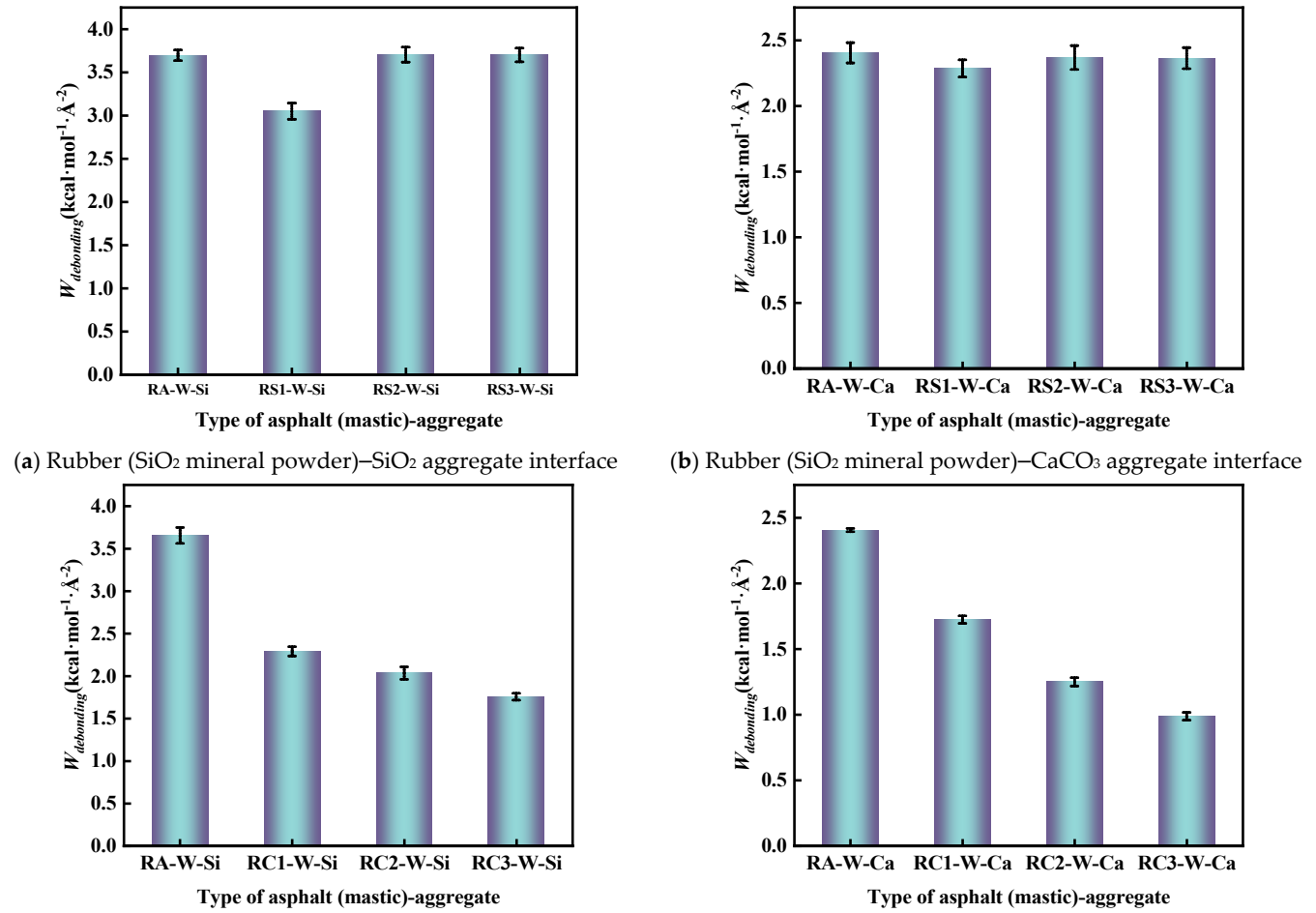

(**a**) Rubber (SiO_2 mineral powder)–SiO_2 aggregate interface (**b**) Rubber (SiO_2 mineral powder)–$CaCO_3$ aggregate interface

(**c**) Rubber ($CaCO_3$ mineral powder)–SiO_2 aggregate interface (**d**) Rubber ($CaCO_3$ mineral powder)–$CaCO_3$ aggregate interface

Figure 18. Debonding work of the rubber asphalt (mastic)–aggregate.

From Figure 18, it is found that the addition of SiO_2 and $CaCO_3$ fillers can effectively reduce the debonding work between rubber asphalt–aggregate. For example, the debonding work of RA–W–Si, RS1–W–Si, and RC1–W–Si was 3.66 kcal·mol^{-1}·Å^{-2}, 3.12 kcal·mol^{-1}·Å^{-2}, and 2.29 kcal·mol^{-1}·Å^{-2}, respectively. This indicates that SiO_2 and $CaCO_3$ fillers can improve the moisture damage resistance of rubber asphalt. However, SiO_2 fillers are very limited in improving the ability of rubberized asphalt to resist moisture damage. This is because the surface of $CaCO_3$ particles has positive and negative charges. The electronegative atoms (N, S, and O) present in both the crumb rubber and asphalt binder generate substantial electrostatic attraction forces. This molecular-level interaction enables rubber-modified asphalt to maintain strong interfacial bonding with aggregates even under moisture-exposed conditions. Furthermore, $CaCO_3$ particles exhibit high surface energy and pronounced hydrophilicity, enabling them to establish robust interfacial

interactions with both asphalt and water molecules. A portion of water molecules become adsorbed onto the $CaCO_3$ particle surfaces, forming a structured water film that effectively inhibits further water molecule diffusion (Figure 19). These synergistic effects collectively enhance the interfacial stability, thereby significantly improving the moisture damage resistance of rubber-modified asphalt systems.

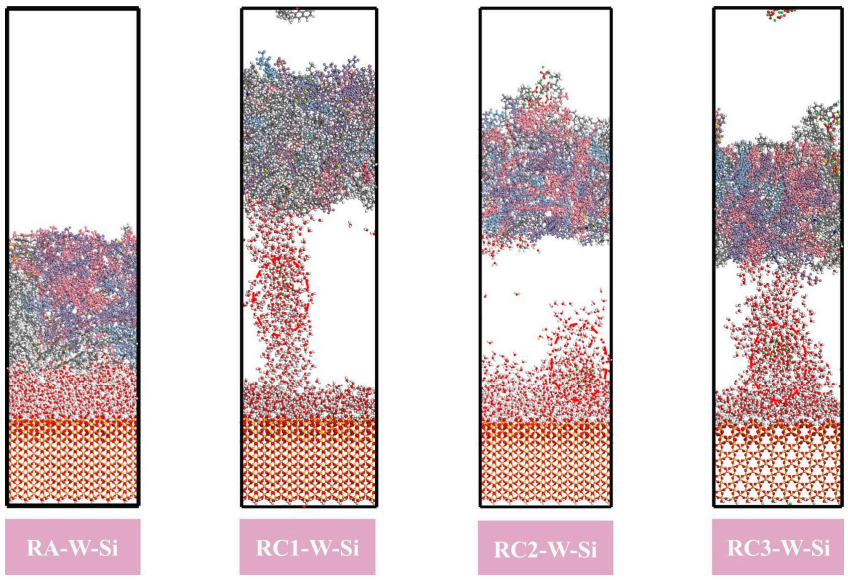

(**a**) Rubber ($CaCO_3$ mineral powder) asphalt mastic–water–SiO_2 aggregate interfacial conformation

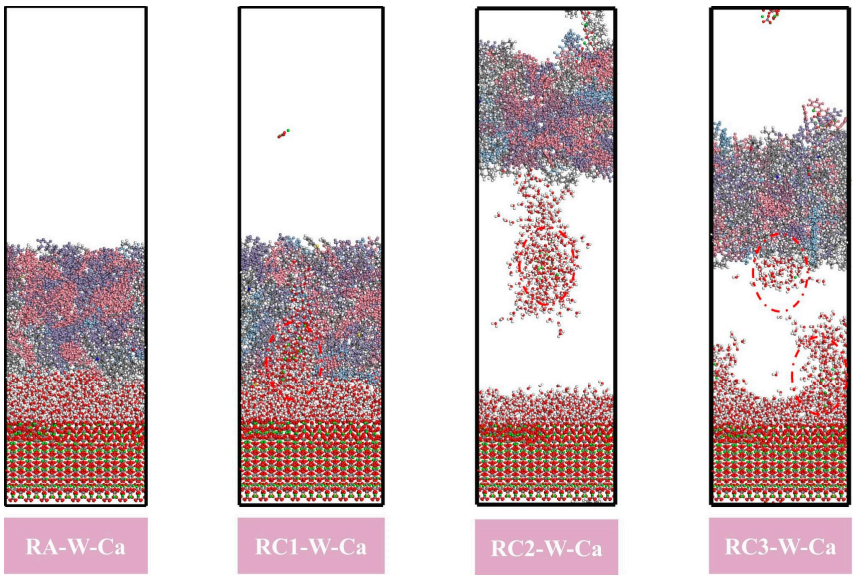

(**b**) Rubber ($CaCO_3$ mineral powder) asphalt mastic–water–$CaCO_3$ aggregate interfacial conformation

Figure 19. Rubber asphalt mastic–water–aggregate interfacial conformation.

However, for SiO_2 particles, the SiO_2 surface relies on van der Waals forces to interact with asphalt and water molecules, and these forces are easily interfered with and weakened by water molecules. In addition, due to the lack of electrostatic forces, SiO_2 is unable to provide sufficiently strong interfacial bonding in the presence of water, making it easier for water molecules to penetrate into the interface, thus reducing the resistance to moisture damage. This is attributed to the fact that the weak electrical properties of SiO_2 cause water molecules to collect between the rubber asphalt mastic and the aggregate, forming a thick water film, as shown in Figure 20. This water film forms an isolation layer between rubber asphalt mastic and aggregate, weakening the bond between rubber asphalt and aggregate.

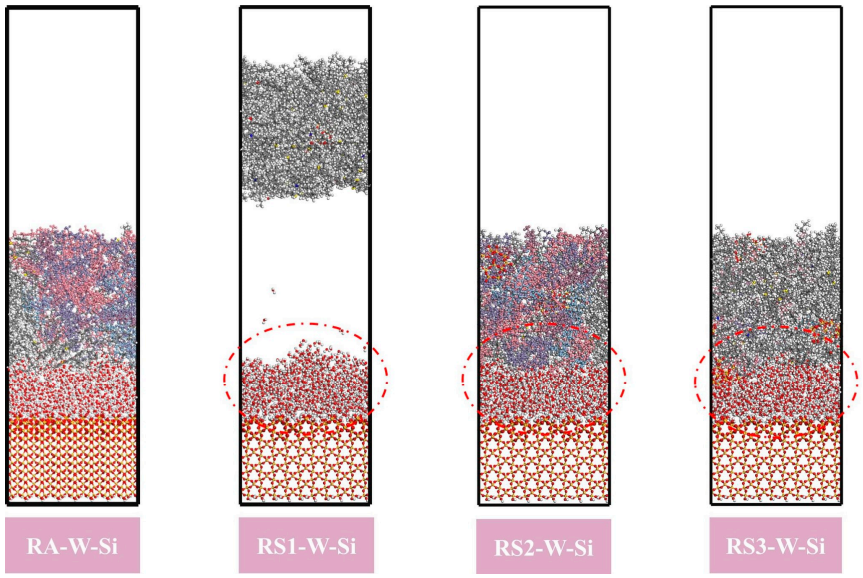

(**a**) Rubber (SiO_2 mineral powder) asphalt mastic–water–SiO_2 aggregate interfacial conformation

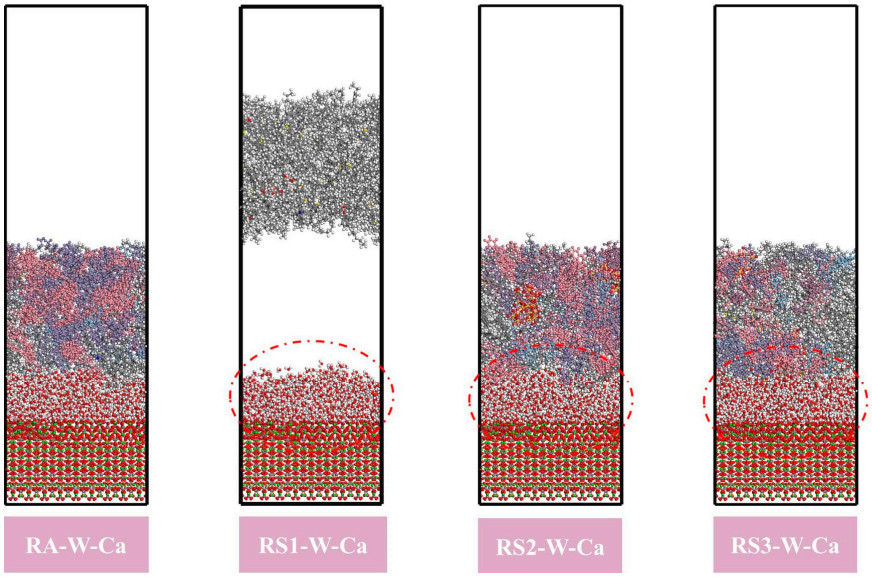

(**b**) Rubber (SiO_2 mineral powder) asphalt mastic–water–$CaCO_3$ aggregate interfacial conformation

Figure 20. Rubber asphalt mastic–water–aggregate interfacial conformation.

4.5. Energy Ratio Between Asphalt and Aggregate

The energy ratio (ER) is a comprehensive parameter that characterizes the bonding and debonding behavior between rubberized asphalt mastic and aggregate, and the ER values of rubberized asphalt mastic and aggregate were calculated using Equation (7), and the results are shown in Figure 21.

In Figure 21, the ER values of rubber asphalt mastic–SiO_2 aggregate were lower than those of rubber asphalt mastic–$CaCO_3$ aggregate. A similar result can be found in previous studies [43]. For example, the ER values for RS1–Si and RS1–Ca are 6.59% and 12.01%. The type of mineral powder greatly affects the ER value of rubber asphalt mastic–aggregate, as shown in Figure 21. The ER values for RS1–Si and RC1–Si were 6.59% and 18.42%, respectively. The ER values for RS1–Ca and RC1–Ca were 12.01% and 77.85%, respectively. This indicates that the debonding of rubberized asphalt–aggregate by $CaCO_3$ mineral powder is much better than the debonding of rubber asphalt–aggregate by SiO_2 mineral powder. In addition, the rubber asphalt mastic–$CaCO_3$ aggregate has better anti-debonding

properties with the synergistic effect of $CaCO_3$ mineral powder and $CaCO_3$ aggregate. This property is one of the factors why limestone is often used as a road building material.

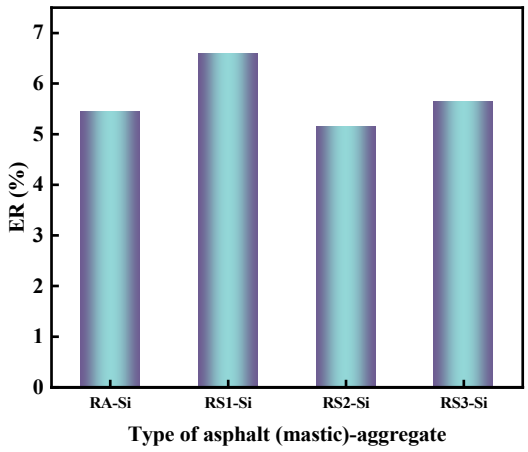

(**a**) Rubber (SiO_2 mineral powder)–SiO_2 aggregate interface

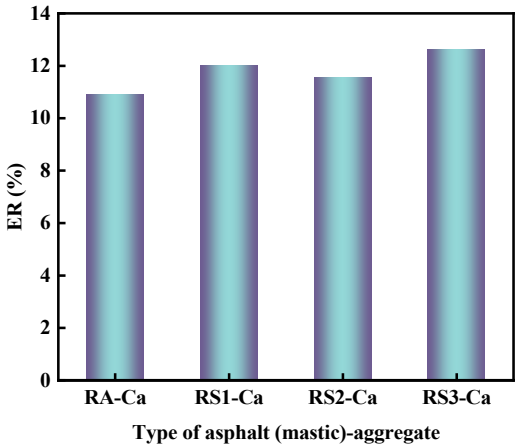

(**b**) Rubber (SiO_2 mineral powder)–$CaCO_3$ aggregate interface

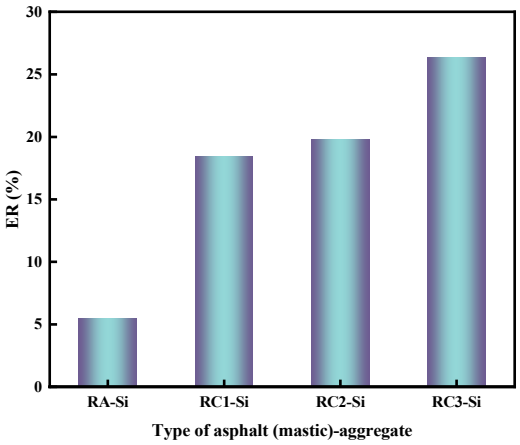

(**c**) Rubber ($CaCO_3$ mineral powder)–SiO_2 aggregate interface

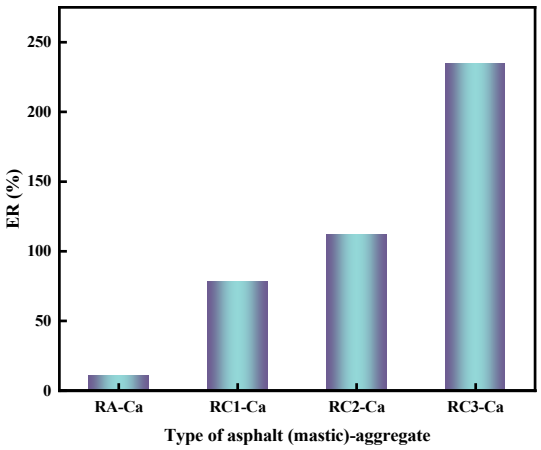

(**d**) Rubber ($CaCO_3$ mineral powder)–$CaCO_3$ aggregate interface

Figure 21. ER of rubber asphalt (mastic)–aggregate.

5. Conclusions

This work investigated the adhesion properties and debonding behavior between rubber asphalt (mastic) and aggregate using surface free energy theory and molecular dynamics. Some key conclusions were drawn:

(1) Limestone mineral powder enhances the surface energy and dispersive component of asphalt and reduces the polar component of asphalt. It improves the adhesion work between rubber asphalt and aggregate and inhibits water molecules from displacing the asphalt film between rubber asphalt and aggregate.

(2) The type of mineral powder has a significant effect on the interaction energy between rubber asphalt–aggregate. The interaction energy between rubber asphalt/SiO_2–aggregate is dominated by van der Waals forces, and the interaction energy between rubber asphalt/$CaCO_3$–aggregate is dominated by electrostatic forces.

(3) Mineral powder plays three important roles between rubber asphalt mastic and aggregate, and they are to (a) promote rubber asphalt mastic to fill the void on the surface of aggregate, (b) form a cluster structure with asphalt molecules in asphalt to increase the direct contact area between rubber asphalt and aggregate, and (c) act as a bridge between rubber asphalt and aggregate.

(4) $CaCO_3$ clusters form a cluster structure with water molecules and reduce the water film thickness between rubber asphalt–aggregate. On the contrary, SiO_2 clusters do not change the water film thickness between rubber asphalt–aggregate. The synergistic effect of the $CaCO_3$ cluster structure and $CaCO_3$ aggregate layer resulted in good adhesion characteristics and an anti-debonding effect of rubber/$CaCO_3$ asphalt mastic–$CaCO_3$ aggregate.

(5) While this study elucidates the fundamental mechanisms governing rubber asphalt–aggregate adhesion, several promising directions warrant further investigation: (1) extending the current framework to hybrid filler systems (e.g., $CaCO_3$–SiO_2 composites) to optimize synergistic effects; (2) evaluating long-term durability under coupled environmental–mechanical aging (UV/oxidation, freeze–thaw cycles, and traffic loading); (3) developing multiscale models bridging molecular interactions to macroscopic performance; and (4) exploring sustainable functionalization of fillers (e.g., nano-$CaCO_3$ or bio-based modifiers) to enhance interfacial stability. Such advances would accelerate the design of high-performance rubber asphalt mixtures with tailored adhesion properties for diverse climatic and loading conditions.

Author Contributions: Conceptualization, H.Y. and X.W.; methodology, S.C.; software, S.C.; formal analysis, F.G.; investigation, F.G.; resources, S.C.; data curation, F.G.; writing—original draft preparation, H.Y.; writing—review and editing, S.C.; supervision, F.G. All authors have read and agreed to the published version of the manuscript.

Funding: This research received no external funding.

Institutional Review Board Statement: Not applicable.

Informed Consent Statement: Not applicable.

Data Availability Statement: The original contributions presented in this study are included in the article. Further inquiries can be directed to the corresponding authors.

Conflicts of Interest: Author Shenyang Cao was employed by the company Gansu New Development Investment Group Ltd. The remaining authors declare that the research was conducted in the absence of any commercial or financial relationships that could be construed as a potential conflict of interest.

References

1. Selsal, Z.; Karakas, A.S.; Sayin, B. Effect of pavement thickness on stress distribution in asphalt pavements under traffic loads. *Case Stud. Constr. Mater.* **2022**, *16*, e01107. [CrossRef]
2. Germin-Aizac, J.; Maitre, A.; Balducci, F.; Montlevier, S.; Marques, M.; Tribouiller, J.; Demeilliers, C.; Persoons, R. Bitumen fumes and PAHs in asphalt road paving: Emission characteristics, determinants of exposure and environmental impact. *Environ. Res.* **2023**, *228*, 115824. [CrossRef] [PubMed]
3. Jiang, Q.; Chen, M.; Zhao, Y.; Wu, S.; Fan, Y.; Gan, Z.; Zhang, Y. Comprehensive assessment of the durability deterioration of asphalt pavement in salt environment: A literature review. *Case Stud. Constr. Mater.* **2022**, *17*, e01706. [CrossRef]
4. Malinowski, S.; Woszuk, A.; Franus, W. Modern two-component modifiers inhibiting the aging process of road bitumen. *Constr. Build. Mater.* **2023**, *409*, 133838. [CrossRef]
5. Guo, D.; Yang, S.; Xu, M.; Li, X.; Sun, X.; Wang, T.; An, Y.; Huang, S. Preparation and performance study of PPA-REOB composite modified bitumen. *Constr. Build. Mater.* **2025**, *468*, 140361. [CrossRef]
6. Kazemian, M.; Raeisi, E.H.; Ghezelhesar, A.D.; Hajimirzajan, A.; Fischer, S. Effects of Crumb Rubber-Modified Asphalt as a Pavement Layer in Railways: A Scoping Review. *Infrastructures* **2025**, *10*, 84. [CrossRef]
7. Hosseinnezhad, S.; Kabir, S.F.; Oldham, D.; Mousavi, M.; Fini, E.H. Surface functionalization of rubber particles to reduce phase separation in rubberized asphalt for sustainable construction. *J. Clean. Prod.* **2019**, *225*, 82–89. [CrossRef]
8. Picado-Santos, L.G.; Capitão, S.D.; Neves, J.M.C. Crumb rubber asphalt mixtures: A literature review. *Constr. Build. Mater.* **2020**, *247*, 118577. [CrossRef]
9. Lyu, L.; Fini, E.H.; Pei, J.; Poulikakos, L.D. Aging evolution and sustainability implications of crumb rubberized asphalt binder: A state-of-the-art. *J. Clean. Prod.* **2024**, *434*, 140202. [CrossRef]

10. Li, J.; Jiang, H.; Han, F.; Lin, Z.; Zhao, Z.; Jin, X.; Liu, Y. Investigation of the effects of chemical modification and oxidative aging on the properties and compatibility of rubber asphalt based on thermodynamic principles. *J. Clean. Prod.* **2023**, *428*, 139070. [CrossRef]
11. Guo, F.; Pei, J.; Huang, G.; Zhang, J.; Falchetto, A.C.; Korkiala-Tanttu, L. Investigation of the adhesion and debonding behaviors of rubber asphalt and aggregates using molecular dynamics simulation. *Constr. Build. Mater.* **2023**, *371*, 130781. [CrossRef]
12. Xie, T.; He, Z.; Yu, H.; Ma, Y.; Shi, C.; Zhang, C.; Ge, J.; Dai, W. Evaluation of styrene butadiene rubber asphalt modification mechanism and adhesion effect based on molecular simulation. *Fuel* **2024**, *364*, 131023. [CrossRef]
13. Li, N.; Wang, J.; Si, W.; Hu, D. Quantitative analysis of adhesion characteristics between crumb rubber modified asphalt and aggregate using surface free energy theory. *Materials* **2022**, *15*, 5735. [CrossRef] [PubMed]
14. Zhang, L.; Long, N.; Liu, Y.; Wang, L. Cross-scale study on the influence of moisture-temperature coupling conditions on adhesive properties of rubberized asphalt and steel slag. *Constr. Build. Mater.* **2022**, *332*, 127401. [CrossRef]
15. Jiao, B.; Chen, J.; Gong, M. Investigation of interfacial degradation mechanism and debonding behavior for degraded rubber asphalt-aggregate molecular system using a molecular dynamics method. *J. Clean. Prod.* **2024**, *451*, 142123. [CrossRef]
16. Chen, Z.; Huang, G.; Wang, S.; Wang, X.; Wang, Z.; Zhang, J.; Falchetto, A.C. Variation of SARA fractions of crumb rubber modified asphalt binder-aggregate interface system and its correlation with adhesion properties. *Constr. Build. Mater.* **2024**, *435*, 136902. [CrossRef]
17. Mohamed, A.S.; Xiao, F.; Hettiarachchi, C.; Abdel-Wahed, T. Bond strength in dry condition of reclaimed asphalt modified by crumb rubber modified binder. *J. Adhes.* **2023**, *99*, 691–720. [CrossRef]
18. Xu, W.; Qiu, X.; Xiao, S.; Hu, G.; Wang, F.; Yuan, J. Molecular dynamic investigations on the adhesion behaviors of asphalt mastic–aggregate interface. *Materials* **2020**, *13*, 5061. [CrossRef]
19. Tan, Y.; Guo, M. Using surface free energy method to study the cohesion and adhesion of asphalt mastic. *Constr. Build. Mater.* **2013**, *47*, 254–260. [CrossRef]
20. Zhang, J.; Shen, Q.; Ji, P.; Wang, J.; Xiao, Y. Influence of filler type and rheological properties of asphalt mastic on the asphalt mastic–aggregate interaction. *Materials* **2023**, *16*, 574.
21. Men, B.; Guo, F.; Kang, X.; Yue, J. Research on the Adhesion Properties of Fast-Melting SBS-Modified Asphalt–Aggregate Based on Surface Free Energy Theory. *Materials* **2023**, *16*, 7601. [CrossRef] [PubMed]
22. Shi, Z.; Min, Z.; Chen, F.; Huang, W. Adhesion behavior and microscopic mechanism of epoxy asphalt-RAP aggregate interface. *Constr. Build. Mater.* **2024**, *457*, 139361. [CrossRef]
23. Shi, C.; Ge, J.; Yu, H.; Qian, G.; Zhou, H.; Ma, Y.; Nian, T.; Yao, D.; Wang, Y.; Zhong, Y. Interfacial adhesion properties and debonding mechanisms in rejuvenated asphalt mixtures. *Constr. Build. Mater.* **2024**, *425*, 135973. [CrossRef]
24. Wang, L.; Chen, L.; Li, Y.X.; Guan, H.F.; Jing, M. Adhesion Characteristics of Warm-Mix Crumb Rubber-Modified Asphalt-Steel Slag Interface under Water Erosion. *J. Mater. Civ. Eng.* **2024**, *36*, 04024270. [CrossRef]
25. Ji, H.; Li, B.; Yao, T.; Liu, Z.; Han, J.; Li, A. Polyurethane and nano-TiO2 modifiers mitigate aging of asphalt binders by inhibiting aggregation of polar molecules: A molecular dynamics study. *Colloids Surf. A Physicochem. Eng. Asp.* **2023**, *679*, 132654. [CrossRef]
26. Yaphary, Y.L.; Leng, Z.; Wang, H.; Ren, S.; Lu, G. Characterization of nanoscale cracking at the interface between virgin and aged asphalt binders based on molecular dynamics simulations. *Constr. Build. Mater.* **2022**, *335*, 127475. [CrossRef]
27. Wang, L.; Zhang, L.; Liu, Y. Molecular dynamics study on the effect of mineral composition on the interface interaction between rubberized asphalt and aggregate. *J. Mater. Civ. Eng.* **2022**, *34*, 04022032. [CrossRef]
28. Yu, H.; Ge, J.; Qian, G.; Zhang, C.; Dai, W.; Li, P. Evaluation on the rejuvenation and diffusion characteristics of waste cooking oil on aged SBS asphalt based on molecular dynamics method. *J. Clean. Prod.* **2023**, *406*, 136998. [CrossRef]
29. Hu, K.; Yu, C.; Chen, Y.; Li, W.; Wang, D.; Zhang, W. Multiscale mechanisms of asphalt performance enhancement by crumbed waste tire rubber: Insight from molecular dynamics simulation. *J. Mol. Model.* **2021**, *27*, 170. [CrossRef]
30. Jiao, B.; Pan, B.; Liu, F.; Yin, P.; Li, Z. Evaluating the interfacial properties between crumb rubber modified asphalt and aggregates using molecular dynamics simulation methods. *Constr. Build. Mater.* **2023**, *400*, 132809. [CrossRef]
31. Han, J.; Li, B.; Ji, H.; Guo, F.; Wei, D.; Cao, S.; Zhang, W.; Chen, X. Interfacial adhesion between recycled asphalt binder and aggregates considering aggregate surface anisotropy: A molecular dynamics simulation. *Constr. Build. Mater.* **2024**, *438*, 137176. [CrossRef]
32. Liu, K.; Yang, Q.; Qiu, X.; Xu, W.; Xiao, S.; Gu, Y.; Ye, Y. An investigation toward adhesion characteristics of emulsified asphalt residue–aggregate interface through MD simulation. *Constr. Build. Mater.* **2024**, *438*, 137251. [CrossRef]
33. Meng, Y.J.; Lai, J.; Mo, S.Y.; Fang, G.; Deng, S.; Wei, X.; Yang, F. Investigating the deterioration mechanism of adhesion between asphalt and aggregate interface under acid rain erosion. *Appl. Surf. Sci.* **2023**, *639*, 158171. [CrossRef]
34. Tang, Y.; Fu, Z.; Ma, F.; Zhao, P.; Hou, Y.; Jiang, X.; Peng, C. Effect of water molecular behavior on adhesion properties of asphalt-aggregate interface. *Constr. Build. Mater.* **2023**, *402*, 133028. [CrossRef]

35. Zou, Y.; Gao, Y.; Chen, A.; Wu, S.; Li, Y.; Xu, H.; Wang, H.; Yang, Y.; Amirkhanian, S. Adhesion failure mechanism of asphalt-aggregate interface under an extreme saline environment: A molecular dynamics study. *Appl. Surf. Sci.* **2024**, *645*, 158851. [CrossRef]
36. Dan, L.; Chuanfeng, Z.; Yong, Q.; Heng, B.; Keyao, L.; Junfei, H. Analysing the effects of the mesoscopic characteristics of mineral powder fillers on the cohesive strength of asphalt mortars at low temperatures. *Constr. Build. Mater.* **2014**, *65*, 330–337. [CrossRef]
37. Wang, F.; Xiao, Y.; Chen, Z.; Cui, P.; Liu, J.; Wang, N. Morphological characteristics of mineral filler and their influence on active adhesion between aggregates and bitumen. *Constr. Build. Mater.* **2022**, *323*, 126520. [CrossRef]
38. Pasandín, A.R.; Pérez, I. The influence of the mineral filler on the adhesion between aggregates and bitumen. *Int. J. Adhes. Adhes.* **2015**, *58*, 53–58. [CrossRef]
39. Yu, H.; Ge, J.; Qian, G.; Shi, C.; Zhang, C.; Dai, W.; Xie, T.; Nian, T. Evaluation of the interface adhesion mechanism between SBS asphalt and aggregates under UV aging through molecular dynamics. *Constr. Build. Mater.* **2023**, *409*, 133995. [CrossRef]
40. Long, Z.; You, L.; Tang, X.; Ma, W.; Ding, Y.; Xu, F. Analysis of interfacial adhesion properties of nano-silica modified asphalt mixtures using molecular dynamics simulation. *Constr. Build. Mater.* **2020**, *255*, 119354. [CrossRef]
41. Sun, G.; Zhang, J.; Chen, Z.; Niu, Z.; Li, Y. Interfacial performance of asphalt-aggregate system under different conditions based on molecular dynamics simulation. *J. Mater. Civ. Eng.* **2023**, *35*, 04023116. [CrossRef]
42. Malinowski, S.; Woszuk, A.; Wróbel, M.; Makowska, M.; Franus, W.; Zofka, A. Bitumen binders modified with chemically-crosslinked chitosan. *Road Mater. Pavement Des.* **2023**, *24* (Suppl. 1), 3–18. [CrossRef]
43. Gong, Y.; Xu, J.; Yan, E. Intrinsic temperature and moisture sensitive adhesion characters of asphalt-aggregate interface based on molecular dynamics simulations. *Constr. Build. Mater.* **2021**, *292*, 123462. [CrossRef]

Disclaimer/Publisher's Note: The statements, opinions and data contained in all publications are solely those of the individual author(s) and contributor(s) and not of MDPI and/or the editor(s). MDPI and/or the editor(s) disclaim responsibility for any injury to people or property resulting from any ideas, methods, instructions or products referred to in the content.